Photoionization of the H_{2}^{+} ion by ultrashort elliptically polarized laser pulses

Xiaoxu Guan, Ryan C. DuToit, and Klaus Bartschat

Phys. Rev. A **87**, 053410 — Published 22 May 2013

DOI: 10.1103/PhysRevA.87.053410

Photoionization of the H_2^+ ion by ultrashort elliptically polarized laser radiation

Xiaoxu Guan[1], Ryan C. DuToit[1], and Klaus Bartschat[1]
[1]*Department of Physics and Astronomy, Drake University, Des Moines, Iowa 50311, USA*
(Dated: May 1, 2013)

We report calculations for the single- and multi-photon ionization of the H_2^+ molecular ion irradiated by ultrashort elliptically polarized laser pulses for central photon energies ranging from close to the ionization threshold up to 300 eV. Using the fixed-nuclei approximation, the electronic response of the system is obtained through an *ab initio* time-dependent grid-based approach implemented in two-center prolate spheroidal coordinates. The predicted cross sections for single-photon absorption are analyzed in a time-independent framework. A concise decomposition of the cross-section patterns exists in terms of the degrees of linear and circular portions of the elliptically polarized radiation. An asymmetric rotational effect in the photoelectron angular distribution is predicted and discussed according to the above decomposition. The confinement effect, previously seen in angle-resolved cross sections for linearly polarized light, persists for circularly polarized radiation. The dependence of the calculated angular distributions on the pulse length in intense laser fields is also analyzed.

PACS numbers: 33.80.-b, 33.80.Wz, 31.15.A-

I. INTRODUCTION

With the availability of ultrafast intense radiation from free-electron lasers and high-order harmonics generation, photoionization of atoms and molecules by vacuum ultraviolet and x-ray radiation has attracted much interest from both experiment and theory. High-intensity and high-brilliance radiation with photon energies ranging from hundreds to even a few thousands of eV opens up new avenues to explore the fundamental processes in light-matter interaction, including the complete breakup of atomic and molecular targets by single- and multiphoton absorption and the diffraction imaging of biomaterial [1, 2].

Recently, the complete breakup problem of H_2 molecules was experimentally studied [3] by using circularly polarized photons at photon energies of 160 eV and 240 eV with the goal of detecting possible interference fringes in this two-center Coulomb system. Follow-up theoretical work [4] suggested that the classical patterns of double-slit interference in the photoelectron angular distribution (PAD) are only visible at even higher photon energies.

Angular distributions of photoelectrons from the deep inner-shell $1\sigma_g$ and $1\sigma_u$ orbitals have also been measured for N_2 molecules in linearly polarized synchrotron radiation at the high photon energy of 419 eV using the DESK facility [5]. On the theoretical front, double-slit interference effects in light diatomic targets, H_2^+, H_2, and Li_2^+ [6, 7], by circularly polarized laser radiation have been investigated by employing single-center expansions. In our recent works [8, 9], we systematically studied the diffraction patterns of H_2^+ and heteromolecular HeH^{2+} irradiated by high-frequency ultrashort radiation. Linearly polarized laser pulses, whose polarization vector was aligned at various angles with respect to the molecular axis, were previously considered in those works. Here we extend our studies to the temporal response of the H_2^+ ion, initialized from the ground and the first excited state, to the general case of *elliptically* polarized radiation. In particular, we will focus on challenging cases in which the polarization plane contains the molecular axis. [If the molecular axis is perpendicular to the polarization plane, the problem is much simpler due to π_u being the only symmetry to consider for one-photon processes.] Generally speaking, elliptically polarized light can be considered as a mixture of linearly and circularly polarized radiation, with well-defined relative portions and phases. This decomposition allows us to explore the effect of *ellipticity* on the PAD from atoms and molecules, thereby going beyond the case of linear polarization.

It is known that the ellipticity of the driving infrared laser field has a significant effect on the efficiency of high-order harmonic generation in atoms (see [10] and references therein.) Combined with other techniques, this fact was exploited to generate an ultrashort isolated single pulse of 130 attoseconds (1 as $= 10^{-18}$ s) with a central photon energy of 36 eV [11]. The availability of such a short pulse at this photon energy makes the dynamical probing for the motion of outer-shell electron in molecules possible.

Early works by Cohen and Fano [12] and Kaplan and Markin [13] promoted ideas of unveiling the similarity between the classical double-slit interference effect and the photoionization of diatomic molecules in the photon energy regime of a few hundred eV, either through angle-integrated or angle-resolved cross sections. For the H_2^+ ion, these ideas and most recent investigations concentrate on linearly polarized radiation, with a few exceptions in studies carried out, for example, by Fernández *et al.* [6, 7] and by Yuan and Bandrauk [14]. In our recent works [8, 9], we showed that the similarity between photoionization in diatomic molecules and classical double-slit interference is sensitive to the molecular orientation with respect to the direction of the linear polarization vector of the light. The similarity appears to

the largest extent when the molecular axis is oriented perpendicular to the polarization vector.

Looking at the general case of elliptically polarized radiation, however, such a well-defined relative orientation between the polarization vector and the molecular axis does not exist. Specifically, the photoionization by elliptically polarized light is the *dynamically* coupled response from the σ_u, π_u, and other high-order transitions. Therefore, the underlying interplay between the two channels may have a significant effect regarding the similarity of quantum angular distributions and classical two-slit interference.

In the present work, we study the photoionization of the H_2^+ molecular ion from the $1s\sigma_g$ ground state and the first excited $2p\sigma_u$ state by arbitrary elliptically polarized laser radiation. [We will assume that the light is 100% polarized, i.e., it does not contain an unpolarized fraction.] The dynamical response to both short and long laser pulses will be presented. As shown in [15], the strength of a time-dependent grid-based approach lies in its ability to treat multiphoton processes driven by intense short laser pulses in cases where time-independent perturbation theory may no longer be applicable. In addition to single-photon ionization, the above-threshold-ionization (ATI) process for 40-eV laser pulses will also be addressed. Here we will only consider the first peak in the ATI spectrum at a photon energy well above the ionization threshold. The entire ATI spectrum of the H_2^+ ion in tunneling ionization regime will be discussed in a later publication.

The present paper is organized as follows. In Sec. II, we outline the necessary theoretical ingredients in the time-dependent scenario, which can be employed for pulses of both short and long time duration. Furthermore, we sketch a time-independent treatment when applicable. PADs from circularly and elliptically polarized laser pulses are presented in Sec. III. We conclude with a summary in Sec. IV.

II. THEORETICAL FORMALISM

The time-dependent Schrödinger equation (TDSE) of the H_2^+ ion driven by an elliptically polarized laser is solved in two-center prolate spheroidal coordinates. The "radial" ξ and "angular" η spatial coordinates are discretized via a discrete-variable representation (DVR) and combined with the finite-element (FE) technique. We use the dipole length gauge and the fixed-nuclei approximation, in which the internuclear separation distance is fixed at R.

In this coordinate system, the TDSE is written as

$$i\frac{\partial}{\partial t}\Psi(t) = \left\{-\frac{2}{R^2(\xi^2-\eta^2)}\left[\frac{\partial}{\partial\xi}(\xi^2-1)\frac{\partial}{\partial\xi}+\frac{\partial}{\partial\eta}(1-\eta^2)\frac{\partial}{\partial\eta}+\frac{\xi^2-\eta^2}{(\xi^2-1)(\eta^2-1)}\frac{\partial^2}{\partial^2\varphi}-\frac{4\xi}{R(\xi^2-\eta^2)}\right]+\boldsymbol{r}\cdot\boldsymbol{\mathcal{E}}(t)\right\}\Psi(t). \tag{1}$$

Here $\boldsymbol{r}$ is the radius vector measured from the center of the molecule while $\boldsymbol{\mathcal{E}}(t)$ is the electric field of the elliptically polarized laser. The wave function is expanded as [15]

$$\Psi(\xi,\eta,\varphi,t) = \sum_{ijm} b_{ij}^m(\xi,\eta,\varphi)C_{ij}^m(t), \tag{2}$$

in terms of the FE-DVR basis functions $\{b_{ij}^m\}$. The latter are defined on grid points (ξ_i,η_j) for a channel specified by the magnetic quantum number m as

$$b_{ij}^m(\xi,\eta,\varphi) = \frac{1}{\sqrt{2\pi a^3(\xi_i^2-\eta_j^2)^3}} f_i(\xi)g_j(\eta)e^{im\varphi}. \tag{3}$$

Here $a = R/2$ is half the internuclear separation, and φ is the azimuthal angle of the electron coordinates. The DVR bases $f_i(\xi)$ and $g_j(\eta)$ are normalized according to $\langle f_i(\xi)|f_{i'}(\xi)\rangle = \delta_{ii'}/\sqrt{w_i^\xi}$ and $\langle g_j(\eta)|g_{j'}(\eta)\rangle = \delta_{jj'}/\sqrt{w_j^\eta}$. Consequently,

$$\int b_{ij}^m(\xi,\eta,\varphi)b_{i'j'}^{m'}(\xi,\eta,\varphi)a^3(\xi^2-\eta^2)d\xi d\eta d\varphi = \delta_{ii'}\delta_{jj'}\delta_{mm'}. \tag{4}$$

As before [8, 9], the expansion coefficients of the wave function in the FE-DVR method, $C_{ij}^m(t)$, are obtained by propagating the vector corresponding to the initial state in time via a short iterative Lanczos algorithm. Being a grid-based approach, these coefficients have a very transparent meaning: they are proportional to the value of the wave function on the grid points, except for some well-known scale factors. Specifically, for the m-component of the wave function in a given channel, $\Psi^{(m)}(\xi,\eta,t) = \langle e^{im\varphi}/\sqrt{2\pi}|\Psi(t)\rangle$, we have

$$\Psi^{(m)}(\xi,\eta,t)\big|_{\xi_i,\eta_j} = \frac{1}{\sqrt{a^3(\xi_i^2-\eta_j^2)w_i^\xi w_j^\eta}} C_{ij}^m(t) \tag{5}$$

at the predefined grid points $(\xi,\eta) = (\xi_i,\eta_j)$ at any time t. Details about our implementations of the FE-DVR method, in particular regarding the boundary conditions adapted in one- and two-electron molecules, can be found in [15–17].

In this work, we investigate the ionization process of the H_2^+ ion in the general case of elliptically polarized radiation. The polarization vector lies in a plane that contains the molecular axis. For a laser pulse of time duration τ, the electric field in Eq. (1)

is written as $\boldsymbol{\mathcal{E}}(t) = f(t)\boldsymbol{E}(t)$ with an envelope function $f(t) = \sin^2(\pi t/\tau)$ and

$$\boldsymbol{E}(t) = E_0^x \cos(\omega_0 t + \delta_x)\boldsymbol{e}_x + E_0^z \cos(\omega_0 t + \delta_z)\boldsymbol{e}_z. \quad (6)$$

Here ω_0 is the central photon frequency or the photon energy in the atomic units (a.u.). Furthermore, E_0^x, E_0^z, and δ_x, δ_z are the amplitudes and phases of the two components of the electric field. We choose the molecular axis to be oriented along the z-axis. After introducing $\boldsymbol{E}_0 = \mathcal{E}_0\boldsymbol{\epsilon}$ with the polarization vector $\boldsymbol{\epsilon}$, the electric field can be expressed as

$$\boldsymbol{E}(t) = \mathrm{Re}\big[\boldsymbol{E}_0 e^{-i(\omega_0 t+\delta)}\big] = \mathcal{E}_0 \mathrm{Re}\big[\boldsymbol{\epsilon} e^{-i(\omega_0 t+\delta)}\big], \quad (7)$$

in which the real amplitude $\mathcal{E}_0$, phase δ, and polarization vector $\boldsymbol{\epsilon}$ remain to be determined for a specific electric field given by Eq. (6).

We refer to the Appendix for detailed definitions of our notation and the derivation of the *complex* polarization vector for arbitrary cases. Depending on the ratio of the two amplitudes E_0^x/E_0^z and the phase difference $\Delta = \delta_z - \delta_x$, there are three general classes. Namely:

1. *Linearly* polarized light: one of the two amplitudes (E_0^x or E_0^z) vanishes or the phase difference Δ is an integer multiple of $\pm\pi$ (i.e., equivalent to $\Delta = 0$). The alignment angle (θ_N) of the polarization vector with respect to the z axis is determined by $\theta_N = \tan^{-1}(E_0^x/E_0^z)$.
2. *Circularly* polarized light: $E_0^x = E_0^z$ and the phase difference is equivalent to $\pm\pi/2$.
3. *Elliptically* polarized light: If the amplitudes and phase differences do not fall into either of the two cases mentioned above, we have the general case of elliptically polarized light.

A few words regarding the case of $\Delta = \pm\pi/2$, in particular for circularly polarized light, seem appropriate. When the direction of the light propagation is specified, one can describe the temporal rotation of the electric field as clockwise or anticlockwise either from the point of view of the receiver or the light source. This leads to the common notations of left-hand/right-hand circular polarization, or positive/negative helicity [18, 19]. For our present photoionization problems in the dipole approximation, however, it is *unnecessary* to introduce the propagation direction of the light. In the time-dependent scenario, two laser beams with opposite directions of propagation can carry exactly the same electric field at the target. Consequently, only the electric field (or the vector potential) is necessary to describe the quantum photoionization processes. Since the direction of the wave vector is not required, we will refrain from the above terminology. See the Appendix for more details.

Both amplitudes of the electric field contribute to the average peak intensity (I_0) of the laser pulse according to

$$I_0 = \big[(E_0^x)^2 + (E_0^z)^2\big] I_{\mathrm{a.u.}}, \quad (8)$$

where the amplitudes of the electric fields are given in a.u., with 1 a.u. of radiation intensity ($I_{\mathrm{a.u.}}$) corresponding to 3.5095×10^{16} W/cm^2. If the laser is elliptically polarized, we have to specify both amplitudes E_0^x and E_0^z, not just the peak intensity. Different combinations of E_0^x and E_0^z can produce the same average intensity.

In short, the polarization vector is written as

$$\boldsymbol{\epsilon} = \frac{\hat{\boldsymbol{\epsilon}}_R + i\epsilon_I \hat{\boldsymbol{\epsilon}}_I}{\sqrt{1+\epsilon_I^2}} \quad (9)$$

for an elliptically polarized electric field. Here $\hat{\boldsymbol{\epsilon}}_R$ and $\hat{\boldsymbol{\epsilon}}_I$ denote the unit vectors of the real and imaginary parts, respectively, which are orthogonal to each other. The above polarization vector is normalized according to $\boldsymbol{\epsilon} \cdot \boldsymbol{\epsilon}^* = 1$. Similar expressions of $\boldsymbol{\epsilon}$ were used by Manakov *et al.* [20], Starace [21] and their co-workers. However, the direction of the wave vector was explicitly introduced to define $\hat{\boldsymbol{\epsilon}}_I$ in terms of $\hat{\boldsymbol{\epsilon}}_R$.

If we were only interested in the non-perturbative time-dependent treatment of the system, it is not necessary to introduce the complex polarization vectors. In the time-dependent scenario, all the relevant physical information, including the angle-integrated and angle-resolved cross sections, or ionization rates, can be extracted without using the concept of polarization vector. However, perturbation theory may be applicable if the peak intensity is relatively weak and the pulse time duration is sufficiently long. If this is the case, it is instructive to use a perturbative formulation to simplify the analysis of the process. In the present work, we use pulses of both short and long time duration, and hence we require the polarization vector in the perturbative framework.

Investigating the photoionization cross sections for atomic and molecular targets [17, 22] due to a laser field, we showed that it is possible, though far from trivial, to obtain accurate and reliable results extracted from the time-dependent approach [16]. Therefore, comparison with the time-independent treatment, should the latter be applicable, will provide an indication regarding the reliability of our time-dependent approach.

At the end of the time evolution (t_e), the probability density for ionization per unit $d\boldsymbol{k}$ in momentum space, i.e., the momentum distribution is given by

$$\frac{dP_{\mathrm{ion}}}{d\boldsymbol{k}} = \big|\langle \Phi_{\boldsymbol{k}}^{(-)} \big| \Psi(t_e)\rangle\big|^2, \quad (10)$$

where $\Phi_{\boldsymbol{k}}^{(-)}$ is the final continuum state normalized on the momentum scale. Furthermore, the PAD is expanded as

$$\frac{dP_{\mathrm{ion}}}{d\Omega} = \int dk \Big| \sum_{\ell m} (-i)^\ell e^{i\Delta_{\ell m}(k)} \mathcal{Y}_{\ell m}(\boldsymbol{k}) \mathcal{F}_{\ell m}(k) \Big|^2, \quad (11)$$

where $\Delta_{\ell m}(k)$ is the two-center Coulomb phase shift and $\mathcal{Y}_{\ell m}(\boldsymbol{k})$ denotes a prolate spheroidal harmonic, which can be computed effectively [23]. Furthermore, $\mathcal{F}_{\ell m}(k)$ is the partial-wave amplitude in the (ℓ, m) ionization channel. Depending on the number of photons absorbed, the PAD

from elliptically polarized light essentially contains contributions from $\sigma_{g,u}$, $\pi_{g,u}$, $\delta_{g,u}$, other channels, and – most importantly – the interference term between them.

The ionization probability at the end of the laser pulse is given by

$$P_{\rm ion} = \int_0^{k_{\rm max}} dk \mathcal{P}_{\rm ion}(k) = \int_0^{E_{\rm max}} dE \mathcal{P}_{\rm ion}(E), \quad (12)$$

where

$$\mathcal{P}_{\rm ion}(k) = \sum_{\ell m} |\mathcal{F}_{\ell m}(k)|^2 \text{ and } \mathcal{P}_{\rm ion}(E) = \frac{\mathcal{P}_{\rm ion}(k)}{\sqrt{2E}}. \quad (13)$$

Here $\mathcal{P}_{\rm ion}(k)$ and $\mathcal{P}_{\rm ion}(E)$ are the ionization probability densities with respect to the momentum (k) and kinetic energy (E) of the photoelectron. We emphasize that the above formalism is valid not only for single-photon ionization, but also for multiphoton absorption.

As will be discussed below, the relative strengths of the transitions to the σ_u ($m = 0$) and π_u ($m = \pm 1$) channels play a commanding role in the determination of the PAD from elliptically polarized radiation. For a linearly polarized laser, if the molecular axis is neither parallel nor perpendicular to the polarization vector, Eq. (11) takes the same general form as for an elliptically polarized laser. The difference lies in the ionization amplitude $\mathcal{F}_{\ell m}(k)$. In the linear case, the alignment angle θ_N is well defined, and hence the dependence on θ_N for one-photon ionization can be factored out in terms of the ionization amplitudes for the σ_u and π_u channels, respectively.

This straightforward factorization does not exist for elliptically polarized light. For sufficiently long laser pulses at relatively "weak" intensity, however, first-order perturbation theory is valid. If this is the case, then the time-dependent wave function of the system can be written in terms of the field-free eigenstates $\{\Phi_n^{(m)}\}$ as

$$\begin{aligned}\Psi(t) =& \Phi_0 e^{-iE_0 t} + \frac{1}{i} E_0^z \sum\!\!\!\!\!\!\int_n \langle \Phi_n^{(m=0)} | r^{(0)} | \Phi_0 \rangle \Phi_n^{(m=0)} \\ &\times \int_0^t dt' f(t') \cos(\omega_0 t' + \delta_z) e^{i(E_n - E_0)t'} e^{-iE_n t} \\ &- \frac{1}{\sqrt{2}i} E_0^x \sum_{m=\pm 1} \sum\!\!\!\!\!\!\int_n m \langle \Phi_n^{(m)} | r^{(m)} | \Phi_0 \rangle \Phi_n^{(m)} \\ &\times \int_0^t dt' f(t') \cos(\omega_0 t' + \delta_x) e^{i(E_n - E_0)t'} e^{-iE_n t}. \end{aligned} \quad (14)$$

Here $r^{(0)} = z$ and $r^{(\pm 1)} = \mp(x + iy)/\sqrt{2}$. We see that the ionization amplitudes $\mathcal{F}_{\ell m}(k)$ are linearly dependent on the amplitudes of the electric field, E_0^z in the σ_u channel and E_0^x in the π_u channel, respectively. Furthermore, after integrating over the solid angle of the photoelectron, the ionization probability at the end of the pulse can be written as

$$P_{\rm ion} = P_{\rm ion}^{(\parallel)}(E_0^z) + P_{\rm ion}^{(\perp)}(E_0^x). \quad (15)$$

Here $P_{\rm ion}^{(\parallel)}(E_0^z)$ and $P_{\rm ion}^{(\perp)}(E_0^x)$ stand for the ionization probabilities in linearly polarized pulses. One is for the parallel geometry at the electric-field amplitude E_0^z, while the other is for the perpendicular geometry with E_0^x. In other words, the ionization probability due to an arbitrary elliptically polarized pulse is separable into two independent components of linearly polarized light, which is independent of the amplitude ratio E_0^x/E_0^z.

Interestingly, however, this conclusion does not hold for the angle-integrated cross sections. The PAD and the ionization probability can, respectively, be converted to angle-resolved and angle-integrated cross sections as

$$\frac{d\sigma}{d\Omega} = \frac{\omega_0}{I_0} \frac{1}{T_{\rm eff}} \frac{dP_{\rm ion}}{d\Omega} \text{ and } \sigma_{\rm ion} = \frac{\omega_0}{I_0} \frac{P_{\rm ion}}{T_{\rm eff}}, \quad (16)$$

where $T_{\rm eff}$ is the effective interaction time with a temporal laser field for one-photon ionization [15]. For an elliptically polarized pulse, the angle-integrated cross section can be expressed as

$$\sigma_{\rm tot} = \frac{1}{1+\gamma} \sigma_{\rm tot}^{(\parallel)} + \frac{\gamma}{1+\gamma} \sigma_{\rm tot}^{(\perp)}, \quad (17)$$

where $\gamma = (E_0^x/E_0^z)^2$. For the particular case of $\gamma = 1$, we have $\sigma_{\rm tot} = \left[\sigma_{\rm tot}^{(\parallel)} + \sigma_{\rm tot}^{(\perp)}\right]/2$, i.e., the average of the contributions from the parallel and perpendicular geometries due to linearly polarized pulses. Equation (17) indicates that for elliptically polarized light with the same E_0^x and E_0^z, the total cross sections are the same as for circularly polarized radiation.

For the arbitrary case of elliptical polarization, Eq. (17) suggests that the cross section is the sum of the cross sections for the parallel and perpendicular geometries due to linear polarization, modified by the appropriate weight factors. Note, however, that Eq. (17) does not indicate that the cross section depends on the amplitudes of the electric fields. Rather, it shows that the cross section remains unchanged if the ratio γ is the same for different cases, even for a varying peak intensity given in Eq. (8). Furthermore, even if the ellipticity of the electric field $\boldsymbol{E}(t)$ varies, the cross sections may remain unchanged, due to the fact that the parameter γ merely depends on the ratio of the amplitudes, while it is independent of the phase difference.

When the time-independent scenario is valid, the differential cross section (DCS) from the initial state Φ_0 to the final continuum state $\Phi_{\boldsymbol{k}}^{(-)}$ can also be obtained through

$$\frac{d\sigma}{d\Omega} = 4\pi^2 \alpha k \left| \langle \Phi_{\boldsymbol{k}}^{(-)} \left| \boldsymbol{r} \cdot \boldsymbol{\epsilon} \right| \Phi_0 \rangle \right|^2, \quad (18)$$

where $\alpha \simeq 1/137$ is the fine-structure constant. Following Manakov *et al.* [20], we introduce the degrees of linear polarization, $l = (1 - \epsilon_I^2)/(1 + \epsilon_I^2)$, and circular polarization, $\zeta = 2\epsilon_I/(1 + \epsilon_I^2)$, respectively. Then $d\sigma/d\Omega$ can be further decomposed as

$$\frac{d\sigma}{d\Omega} = \frac{d\sigma_0}{d\Omega} + l \frac{d\sigma_l}{d\Omega} + \zeta \frac{d\sigma_{\rm CD}}{d\Omega}. \quad (19)$$

With $c_k \equiv 4\pi^2\alpha k$,

$$\frac{d\sigma_0}{d\Omega} = \frac{c_k}{2}\left[\left|\langle\Phi_{\boldsymbol{k}}^{(-)}|\boldsymbol{r}\cdot\hat{\boldsymbol{\epsilon}}_R|\Phi_0\rangle\right|^2 + \left|\langle\Phi_{\boldsymbol{k}}^{(-)}|\boldsymbol{r}\cdot\hat{\boldsymbol{\epsilon}}_I|\Phi_0\rangle\right|^2\right], \quad (20)$$

$$\frac{d\sigma_l}{d\Omega} = \frac{c_k}{2}\left[\left|\langle\Phi_{\boldsymbol{k}}^{(-)}|\boldsymbol{r}\cdot\hat{\boldsymbol{\epsilon}}_R|\Phi_0\rangle\right|^2 - \left|\langle\Phi_{\boldsymbol{k}}^{(-)}|\boldsymbol{r}\cdot\hat{\boldsymbol{\epsilon}}_I|\Phi_0\rangle\right|^2\right], \quad (21)$$

and

$$\frac{d\sigma_{\rm CD}}{d\Omega} = c_k {\rm Im}\left[\langle\Phi_{\boldsymbol{k}}^{(-)}|\boldsymbol{r}\cdot\hat{\boldsymbol{\epsilon}}_R|\Phi_0\rangle\langle\Phi_0|\boldsymbol{r}\cdot\hat{\boldsymbol{\epsilon}}_I|\Phi_{\boldsymbol{k}}^{(-)}\rangle\right]. \quad (22)$$

Here CD stands for the circular dichroism (see the discussions below.) The light is completely linearly polarized when $\epsilon_I = 0$, which corresponds to $l = 1$ and $\zeta = 0$. On the other hand, we have completely circularly polarized light if $\epsilon_I = \pm 1$, corresponding to $l = 0$ and $\zeta = \pm 1$. Generally, we have $l^2 + \zeta^2 = 1$ for the parameterization of arbitrarily polarized light.

Note that $d\sigma_l/d\Omega$ and $d\sigma_{\rm CD}/d\Omega$ are not the differential cross sections, respectively, for linearly and circularly polarized light. One of the appealing advantages of the aforementioned decomposition of $d\sigma/d\Omega$, however, is based on the fact that for a given orientation of the polarization ellipse (specified by the directions of the major $\hat{\boldsymbol{\epsilon}}_R$ and minor $\hat{\boldsymbol{\epsilon}}_I$ axes), $d\sigma_0/d\Omega$, $d\sigma_l/d\Omega$, and $d\sigma_{\rm CD}/d\Omega$ are predetermined and hence independent of the ellipticity.

For the angle-integrated total cross section, we find

$$\sigma_{\rm tot} = \sigma_0 + l\sigma_l. \quad (23)$$

This equation states that only the degree of linear polarization affects the total cross section $\sigma_{\rm tot}$ in the general case of elliptically polarized light. The CD effect vanishes for $\sigma_{\rm tot}$ (i.e., $\sigma_{\rm CD} = 0$), independent of the ellipticity. This result is due to the degree of circular polarization being a pseudoscalar quantity, and hence the contribution to the angle-differential form (19) vanishes after integration over all angles. For 100% circularly polarized laser, in particular, we then have $\sigma_{\rm tot} = \sigma_0$. Note that Eq. (23) is consistent with Eq. (17) for the general case of an elliptically polarized laser.

In conclusion, the cross section due to elliptical polarization can be classified according to the orientation of the ellipse formed by the electric fields. In our case, circular dichroism can only be observed in the PAD. In Ref. [24], a general parameterization of the PAD for the hydrogen atom in a few-cycle xuv pulse was also obtained. As shown by Manakov, Starace, and co-workers [20, 21, 25], such a decomposition of the cross section also exists for even more complicated processes, for example, double photoionization of atoms. In what follows below, Eq. (19) will be used to analyze the symmetry and/or asymmetry patterns in the PAD.

We emphasize that the above decomposition is valid for single-photon ionization in the perturbative regime. Whether or not the decomposition of the PAD also exist for two-photon processes of the H_2^+ molecular ion in strong laser pulses will be addressed elsewhere.

III. RESULTS AND DISCUSSION

Before presenting our results, we provide some details of the computational aspects. The box of the ξ coordinate is truncated at $\xi_{\rm max} = 400$ in most cases and divided into 160 finite elements. Depending on the kinetic energy of the photoelectron, each finite element of ξ is spanned with 10-20 DVR mesh points. We use an increasingly dense ξ grid of mesh points to depict the fast oscillatory behavior in the wave packet when the kinetic energy of the electron grows. Only a single element is used to discretize the η coordinate with 15 mesh points.

In the present work, "long" laser pulses correspond to time durations of 15 to 20 optical cycles (o.c.). This is sufficiently long to extract the cross sections if the peak intensity is relatively weak. On the other hand, "short" pulses generally last for less than 5 cycles. As mentioned above, the time propagation of the initial state is achieved through a short iterative Lanczos algorithm [26]. We obtain high accuracy and efficiency by choosing about 10 as a typical size of the Krylov space.

In the subsections below, we will separately discuss the electronic response of the H_2^+ molecular ion to laser pulses with circular, linear, and arbitrary elliptical polarization. Special attention will also be given to the effect of the pulse duration, i.e., potential differences in the time-dependent results for the long and short pulses characterized above.

A. Angular distributions for long pulses and weak intensities

We begin with Fig. 1, which depicts a comparison of the angle-resolved cross sections obtained in the time-dependent and time-independent scenarios. The laser pulse is elliptically polarized with a central photon energy of 70 eV. The amplitudes E_0^x and E_0^z are, respectively, 0.01 and 0.0136 a.u., thus yielding a peak intensity of $I_0 = 1 \times 10^{13}$ W/cm^2.

The photoelectron is detected in the polarization plane, which contains the molecular axis. We see excellent agreement between the results obtained in the time-dependent and time-independent formalisms, not only in the shape but also the magnitude on an absolute scale. The phase shift between the two components of the electric fields is $\Delta = \delta_z - \delta_x = 60°$. These well-defined cross sections do not depend on the individual phases, δ_z and δ_x, but only on the phase difference Δ. In the time-dependent scenario, different combinations of δ_x and δ_z for a fixed Δ correspond to different initial positions on the same ellipse formed by the resulting electric field, i.e., a carrier envelope phase (CEP) effect. For long and relatively weak pulses, the magnitude and shape of the differential cross sections should not depend on the CEP. As will be demonstrated in the next subsection, however, the magnitude and preferable emission mode in the angular distributions may depend on the CEP for short and

intense pulses.

After solving the TDSE initialized from the $1s\sigma_g$ ground state, we obtain the PADs displayed in Figs. 2 and 3, respectively, at the internuclear separations of 2.0 and 4.0 bohr, in linearly and circularly polarized lasers for photon energies between 40 eV and 300 eV. For the circularly polarized radiation, we set the peak intensity to 2×10^{13} W/cm^2, corresponding to amplitudes $E_0^x = E_0^z = 0.01688$ a.u. for the electric field. We have linearly polarized light when only one component of the electric field, either E_0^x or E_0^z, is kept while the other is set to zero. Holding the amplitudes of the electric field fixed to the components of the circularly polarized laser yields a peak intensity of 1×10^{13} W/cm^2 for linearly polarized radiation.

To begin the discussion, we first note that the dominant emission mode for a photon energy of 40 eV in circularly polarized laser at $R = 2.0$ bohr is oriented along the direction perpendicular to the molecular axis. The dipole transition to the π_u channel is much stronger than that to the σ_u channel for this particular internuclear separation. At $R = 4.0$ bohr, on the other hand, the transition to the σ_u channel overwhelms the π_u channel. Specifically, our calculated integrated cross sections are $\sigma^{(\parallel)} = 38.95$ kb and $\sigma^{(\perp)} = 0.5285$ Mb at $R = 2.0$ bohr, while we obtain $\sigma^{(\parallel)} = 0.4139$ Mb and $\sigma^{(\perp)} = 0.2848$ Mb, respectively, at $R = 4.0$ bohr. Consequently, the dominant mode of emission at $R = 4.0$ bohr is along the molecular axis for circularly polarized radiation. At the higher photon energies, the transition strengths to the σ_u and π_u channels are nearly the same and neither one of them is negligible [c.f. Fig. 3].

In contrast to linearly polarized light (both parallel and perpendicular geometries), the angular distributions clearly show an asymmetric pattern with respect to the molecular axis for circular polarization. For near-threshold ionization, in particular, the circularly polarized radiation "*rotates*" the dominant emission angle for the photoelectron, thus causing a deviation from the pattern seen with linearly polarized light. We call this phenomenon the "*rotational effect*" in the PAD. We observe this rotation only for the dominant emission mode. For example, at $R = 2.0$ bohr and $\hbar\omega_0 = 40$ eV [c.f. Fig. 2], the dominant direction of electron emission is along the direction perpendicular to the molecular axis, but it rotates by a noticeable angle. On the other hand, for the same photon energy but the larger internuclear separation of $R = 4.0$ bohr [c.f. Fig. 3], the electron is preferably emitted along the molecular axis, but again with a non-zero rotation angle. This also indicates that the cross section patterns are *not* symmetric with respect to the plane perpendicular to the polarization plane that contains the molecular axis. Note that the rotational effect disappears for photon energies well above the ionization threshold, effectively when the photon energy exceeds about 150 eV. A similar rotational effect for the same system was also noticed in Ref. [14].

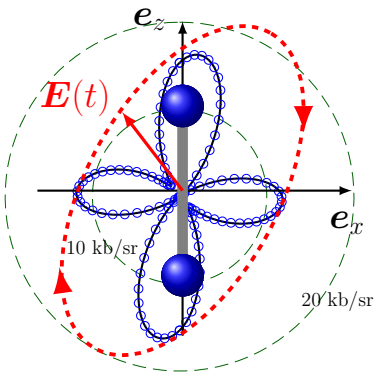

FIG. 1. (Color online) Coplanar differential cross section for photoionization of the H_2^+ molecular ion from the initial ground $1s\sigma_g$ state by a 20-cycle elliptically polarized laser pulse with a central photon energy of 70 eV and peak intensity 1×10^{13} W/cm^2. The solid line represents the differential cross section extracted from the time-dependent formalism, while the circles are the time-independent results. The internuclear separation is $R = 2.0$ bohr. [1 kb $= 1 \times 10^{-21}$ cm^2.]

The above observations can be explained in terms of the decomposition of the cross section pattern. For circularly polarized lasers, the rotational effect in the differential cross sections, if it appears, is related to the phase difference in the electric field components. The DCSs shown in Figs. 2 and 3 correspond to $\Delta = -\pi/2$. Figure 4 displays the DCSs at photon energies of 40 eV and 200 eV for both $\Delta = +\pi/2$ and $-\pi/2$, in which the electric fields rotates, respectively, clockwise and anticlockwise [see the Appendix.] Equation (19) reveals that $d\sigma/d\Omega = d\sigma_0/d\Omega + d\sigma_{\rm CD}/d\Omega$ for $\Delta = -\pi/2$ (i.e., $\xi = +1$) and $d\sigma/d\Omega = d\sigma_0/d\Omega - d\sigma_{\rm CD}/d\Omega$ for $\Delta = +\pi/2$ (i.e., $\xi = -1$). Hence $d\sigma_0/d\Omega$ corresponds to a background that is the same for $\Delta = \pm\pi/2$. In other words, the rotational effect vanishes in the averaged DCS, $d\bar{\sigma}/d\Omega = [d\sigma^{(+)}/d\Omega + d\sigma^{(-)}/d\Omega]/2$, for circularly polarized lasers with the two possible temporal rotations of the electric field. The averaged DCS, $d\bar{\sigma}/d\Omega = d\sigma_0/d\Omega$, retrieves the symmetry with respect to the molecular axis and the plane perpendicular to this axis. Further analysis shows that $d\sigma^{(-)}/d\Omega$ can be obtained by mirror reflection (with respect to the plane perpendicular to the polarization plane) from $d\sigma^{(+)}/d\Omega$ and vice versa.

Figure 5 exhibits the effect of the relative $d\sigma_{\rm CD}/d\Omega$, which is defined as $d\sigma_{\rm CD}/d\Omega$ divided by the maximum of $d\sigma/d\Omega$ in a circularly polarized pulse. Apparently, the interference term in $d\sigma_{\rm CD}/d\Omega$ is only important for photon energies near threshold. Its effect on the DCSs at the higher photon energies is negligible. For near-threshold ionization at 40 eV and 70 eV, for example, $d\sigma_{\rm CD}/d\Omega$ contributes about 20-25% of the maximum of $d\sigma/d\Omega$, which makes the rotational effect very noticeable.

For circularly polarized light, we can always choose the major and minor axes perpendicular to and along the

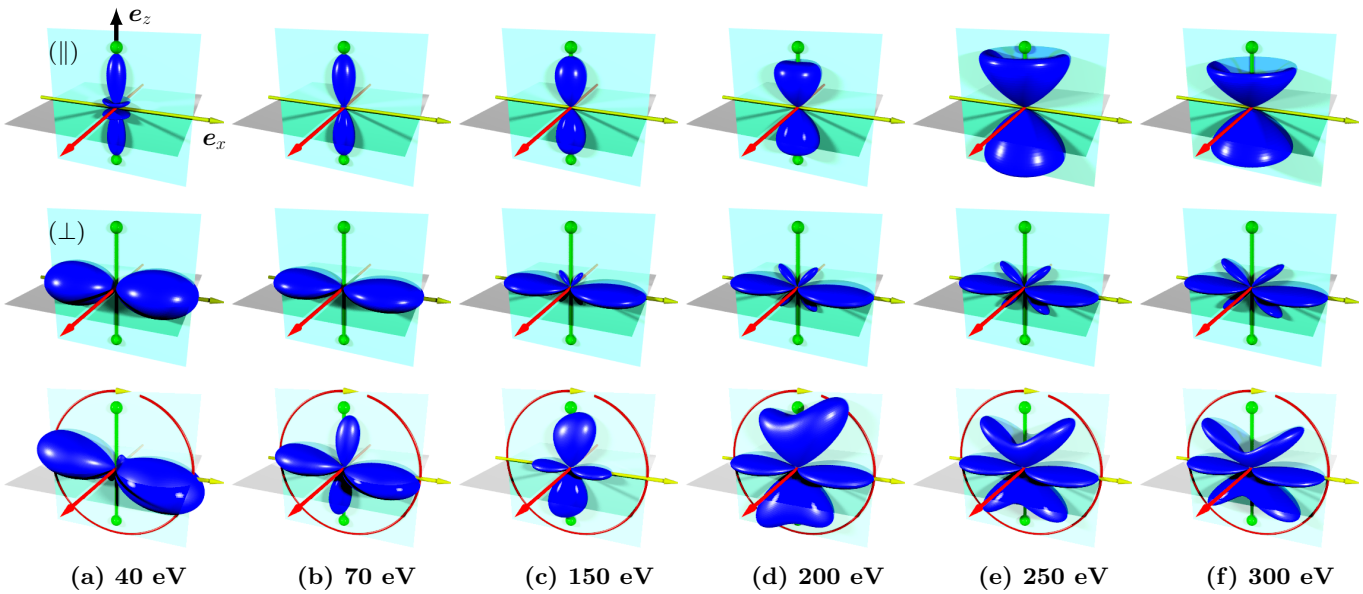

FIG. 2. (Color online) Angular distributions for photoionization of the H_2^+ molecular ion from the initial ground $1s\sigma_g$ state by 15-cycle laser pulses with selected photon energies between 40 eV [panel (a)] and 300 eV [panel (f)]. The molecular axis is along the vertical direction. The first and second rows correspond to the parallel (∥) and perpendicular (⊥) geometries with peak intensities of 1×10^{13} W/cm^2, respectively, while the bottom panels is for circularly polarized radiation with a peak intensity of 2×10^{13} W/cm^2. The circle with the arrow specifies the temporal rotation of the electric field. Note that the angular distributions shown here are not on the same scale. They were rescaled in order to highlight the different angular dependencies. The internuclear separation is $R = 2.0$ bohr.

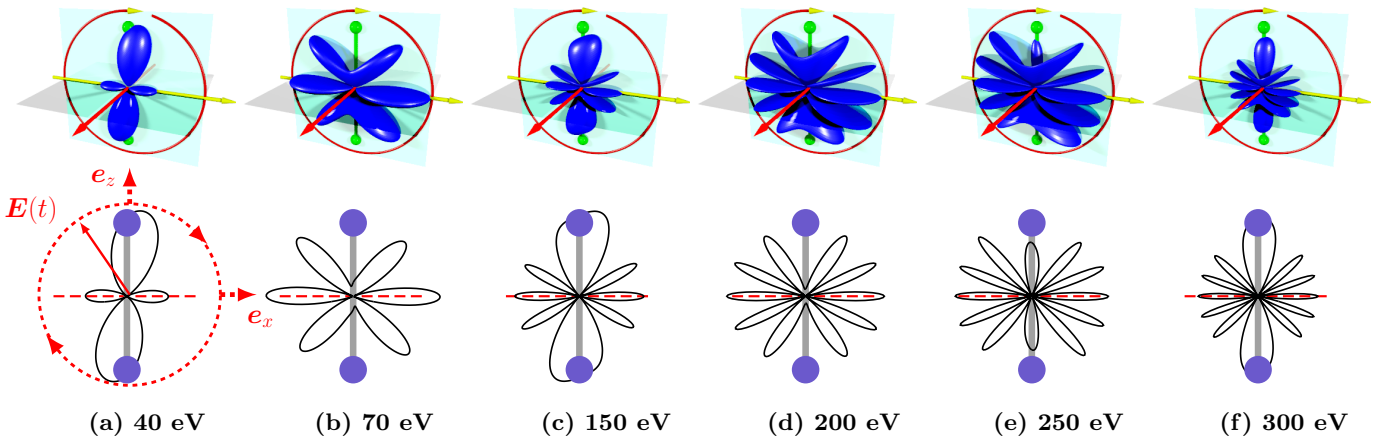

FIG. 3. (Color online) Same as Fig. 2, but only for circularly polarized radiation at $R = 4.0$ bohr. The top panels are the three-dimensional representation, while the bottom panels show the PADs in the polarization plane.

molecular axis, respectively. Further analysis shows that $d\sigma_{\rm CD}/d\Omega$ in this case is proportional to $\sin(2\theta)$, where the angle θ is measured with respect to the molecular axis in the body frame. Hence $d\sigma_{\rm CD}/d\Omega$ vanishes along the directions parallel and perpendicular to the molecular axis [c.f. Fig. 5]. This conclusion is independent of the internuclear separation and the photon energy. The dichroism term is responsible for the asymmetry and the rotational effect in the differential cross section. Circularly polarized radiation generally enhances electron ejection modes away from the molecular axis, in contrast to the parallel and perpendicular geometries with linearly polarized light. [c.f. Fig. 2]. Although the PADs are not symmetric with respect to the molecular axis, the symmetry under the parity inversion $\boldsymbol{k} \to -\boldsymbol{k}$ is preserved.

Another issue to be discussed concerns the so-called "confinement effect". Depending on the particular combination of the internuclear separation and momentum of the photoelectron, the emission mode along the molecular axis may be dynamically suppressed. As seen from Fig. 2, the confinement effect occurs at the same laser parameters for circularly and linearly polarized lasers,

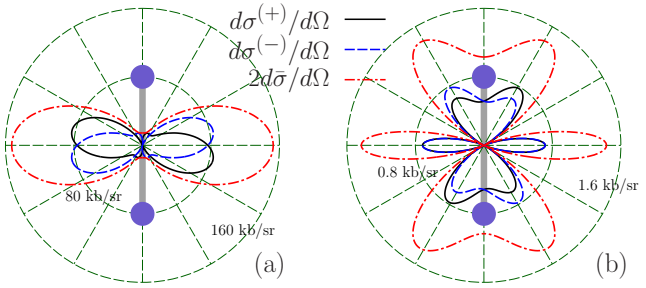

FIG. 4. (Color online) PADs from the H_2^+ molecular ion irradiated by circularly polarized laser light with photon energies of 40 eV (a) and 200 eV (b). $d\sigma^{(+)}/d\Omega$ and $d\sigma^{(-)}/d\Omega$ correspond to $\Delta = +\pi/2$ and $-\pi/2$, respectively, and $2\bar{\sigma}/d\Omega$ is defined as the sum of $d\sigma^{(+)}/d\Omega$ and $d\sigma^{(-)}/d\Omega$. The laser parameters are the same as those of Fig. 2.

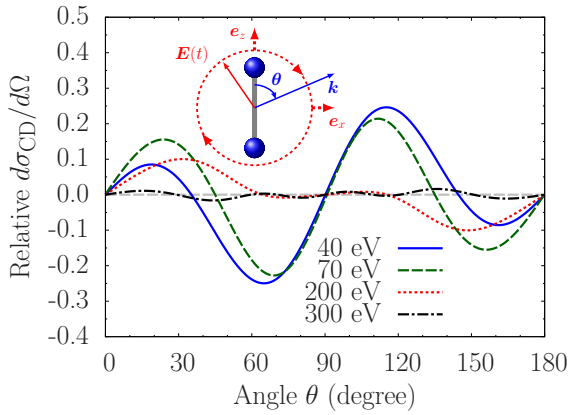

FIG. 5. (Color online) Relative $d\sigma_{\rm CD}/d\Omega$ at photon energies of 40, 70, 200, and 300 eV. The laser parameters are the same as those of Fig. 2.

namely when the condition $kR = n\pi$ (with n being an odd integer) is satisfied. This is not surprising. As explained above, we can choose – without loss of generality – the major and minor axes perpendicular to and along the molecular axis for circularly polarized radiation. The contribution from both the perpendicular component and the dichroism term $d\sigma_{\rm CD}/d\Omega$ must vanish along the molecular axis. Only the parallel component of the electric field contributes to emission along this direction. Consequently, the linear and circular light polarizations share the same condition for the confinement effect.

Figure 6 depicts the angular distributions initialized from the first excited $2p\sigma_u$ state in circularly polarized light. In contrast to the $1s\sigma_g$ initial state, we notice that the ionization probability in the plane perpendicular to the molecular axis is negligibly small for all cases considered here. Note that this is not caused by a selection rule. For circularly polarized radiation, the component of the electric field perpendicular to the molecular axis,

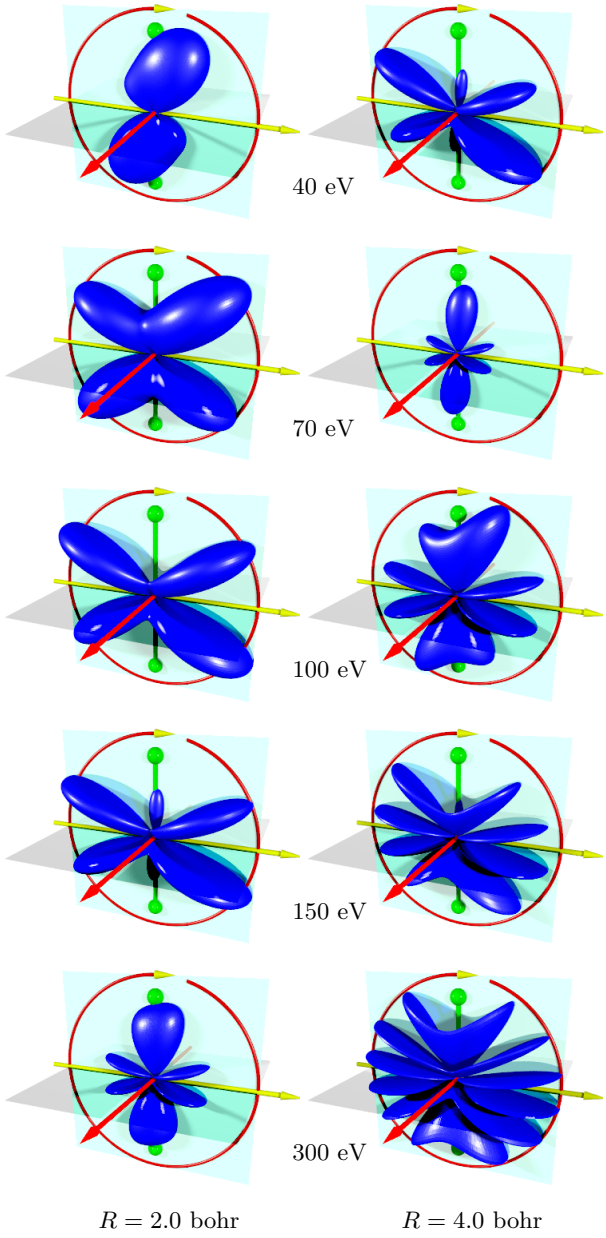

FIG. 6. (Color online) PADs from the excited $2p\sigma_u$ state of the H_2^+ molecular ion by circularly polarized radiation. The photon energies are 40, 70, 100, 150, and 300 eV from top to bottom. Other laser parameters are the same as in Fig. 2. The left and right panels correspond to $R = 2.0$ and 4.0 bohr, respectively.

indeed, forbids emission in this plane. The forbidden mode, however, is broken down by the parallel component, although the probability is small compared to the dominant modes.

Another interesting observation concerns the confinement effect for circular polarizations. The confinement effect is completely different when the process is initialized from the $2p\sigma_u$ state rather than the $1s\sigma_g$ ground state. According to the plane-wave model of Walter and

Briggs [27], the PADs for the σ_g ground state is approximately proportional to $(\boldsymbol{\epsilon}\cdot\boldsymbol{k})^2\cos^2(\boldsymbol{k}\cdot\boldsymbol{R}/2)$, while it becomes $(\boldsymbol{\epsilon}\cdot\boldsymbol{k})^2\sin^2(\boldsymbol{k}\cdot\boldsymbol{R}/2)$ for the initial $2p\sigma_u$ state. For the $2p\sigma_u$ state, therefore, the confinement effect along the molecular axis occurs when the condition $kR = n\pi$ is satisfied, with n as an even integer.

For example, the confinement effect is observed at $R = 4.0$ bohr and photon energies of 150 eV and 300 eV, since $kR = 3.95\pi \simeq 4\pi$ at 150 eV and $kR = 5.79\pi \simeq 6\pi$ at 300 eV. Meanwhile, the emission probability along the molecular axis is very small at 100 eV and $R = 2.0$ bohr. However, the confinement effect is *not* responsible for the pattern at this particular combination of k and R. The de Broglie wavelength in this case is about 2.56 bohr, which is larger than the internuclear separation. Furthermore, we have $kR \simeq 1.56\pi$, which means that the above criterion for the confinement effect is not satisfied. Further analysis shows that in this case the transition probability to the π_g channel is much stronger than that to the σ_g channel. This makes the resulting emission mode along the molecular axis negligibly small. The four-lobe structure in the PAD is mostly from the π_g channel, i.e., from the perpendicular component of the electric field. At the same internuclear separation but a higher photon energy of 300 eV, we obtain a six-lobe structure. In this case, the analysis shows that the dominant emission mode around the molecular axis originates from the σ_g channel, while other off-axis lobes come from the π_g channel. Overall, for the initial σ_g and σ_u states, either a single component or both components of the electric field are responsible for the multi-lobe structure observed in the PAD. The details are very sensitive to the transition strengths to the relevant channels. Finally, the rotational effect is also observed for the initial $2p\sigma_u$ state.

B. Angular distributions for short pulses and high intensities

The angular distributions in our time-dependent method are extracted by projection of the wave packet at the end of the time evolution to the continuum state of the photoelectron. In contrast to the plane-wave approximation, our continuum states $\Phi_{\boldsymbol{k}}^{(-)}(\boldsymbol{r})$ are essentially exact (subject only to numerical issues) eigenstates of the two-center system. Therefore, there is no need to propagate the system for any additional time after the laser pulse is over. We have indeed confirmed that the predicted DCSs are independent of the field-free time evolution in our formalism. This statement is valid for both long and short pulses.

Figure 7 shows the dependence of the coplanar DCS ($d\sigma/d\Omega$) and the angular distribution ($dP_{\rm ion}/d\Omega$) on the time duration of elliptically polarized laser pulses at the weak intensity of 1×10^{13} W/cm^2. For the photon energy of 40 eV, it requires about 10 to 15 o.c. (1.03 to 1.55 fs) to converge the DCS to the time-independent result on an absolute scale. Note, however, that the

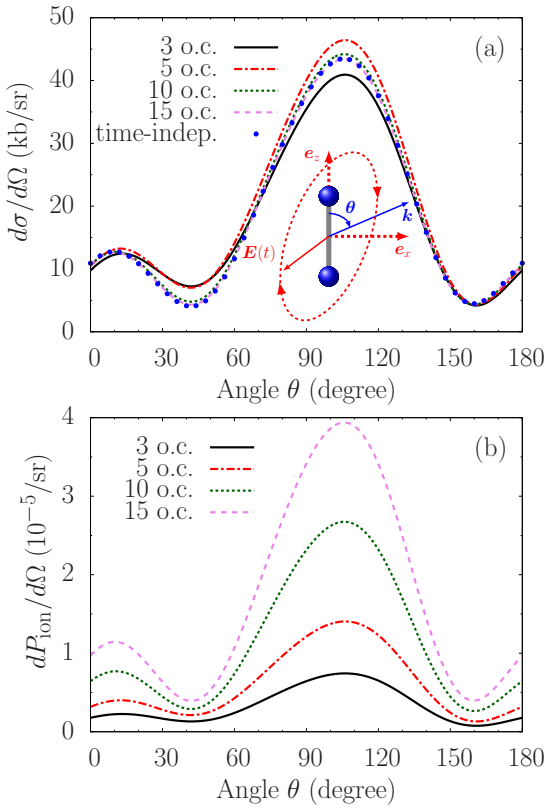

FIG. 7. (Color online) Dependence of the differential cross section $d\sigma/d\Omega$ [panel (a)] and the angular distribution $dP_{\rm ion}/d\Omega$ [panel (b)] on the pulse duration at a central photon energy of 40 eV. The time-independent (time-indep.) DCS is also shown in panel (a). The laser pulses have 3, 5, 10, and 15 optical cycles, and the phase difference is 60°. The amplitudes of the electric field components are $E_0^x = 0.00844$ and $E_0^z = 0.01462$ a.u., corresponding to a peak intensity $I_0 = 1\times10^{13}$ W/cm^2.

DCS does not converge in a uniform fashion. Consistent with the increasing interaction time, the angular distribution $dP_{\rm ion}/d\Omega$ increases in proportion to the pulse length when the time duration is sufficiently long. The phase difference for the DCSs in Fig. 7 is 60°. In the weak-field case, the predicted DCSs are insensitive to the individual phases of δ_x and δ_z, provided the phase difference remains the same. These conditions are essential for the extraction of a meaningful cross section.

On the other hand, ionization driven by 40-eV laser pulses at high intensity around 10^{17} W/cm^2 exhibits very different features compared to the weak-field case. To begin with, multiphoton absorption above the ionization threshold cannot be neglected anymore. High angular-momentum states may provide significant contributions to the ionization events in this multiphoton regime. In Fig. 8, we examine the convergence of the ATI spectrum with respect to the magnetic quantum number (which is not conserved) in elliptically polarized radiation. In our formalism, the total ATI spectrum is represented by

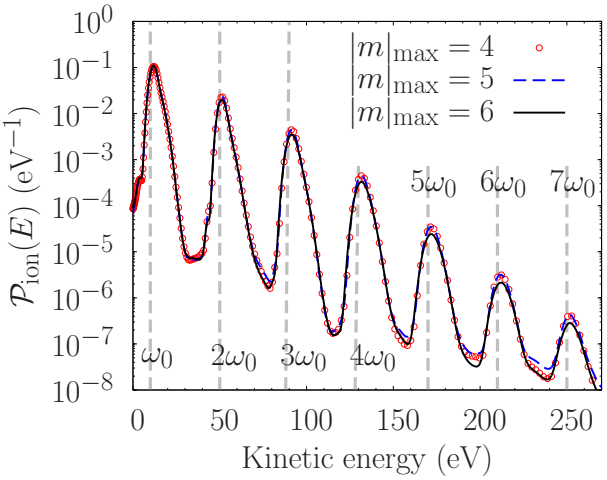

FIG. 8. (Color online) ATI spectrum from the H_2^+ molecular ion exposed to elliptically polarized radiation as a function of the kinetic energy of the photoelectron. The internuclear separation is fixed at $R = 2.0$ bohr. The amplitudes of the electric field components are $E_0^x = 0.844$ and $E_0^z = 1.462$ a.u., corresponding to a peak intensity $I_0 = 1 \times 10^{17}$ W/cm^2. The phase difference is $\Delta = 60°$, the photon energy is 40 eV, and the pulse duration is 15 o.c. The dashed vertical lines indicate the kinetic energy of the photoelectron for n-photon absorption.

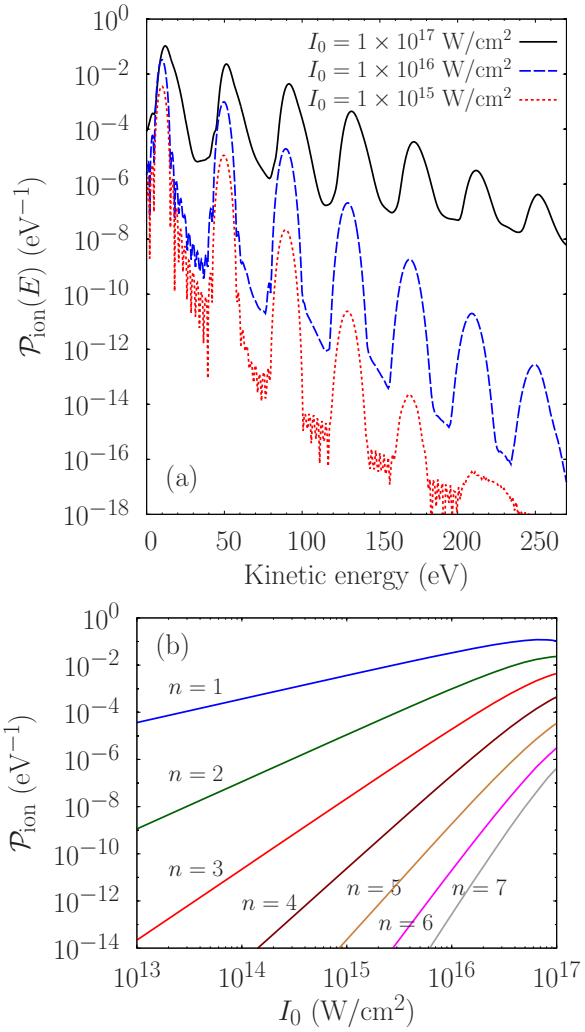

FIG. 9. (Color online) ATI spectrum from the H_2^+ molecular ion exposed to elliptically polarized radiation as a function of the kinetic energy of the photoelectron at the fixed internuclear separation of $R = 2.0$ bohr. The laser parameters are the same as in Fig. 8, except for the peak intensities as indicated. Panel (a) shows the ATI spectrum as a function of the kinetic energy of the photoelectron, while panel (b) displays the peaks of the ATI spectrum for the n-photon absorption as a function of the peak intensity. The ratio of E_0^x and E_0^z is the same as in Fig. 8.

$\mathcal{P}_{\rm ion}(E)$ [c.f. Eq. (12)] after summing over the individual contributions $|\mathcal{F}_{\ell m}(k)|^2$ from all channels. The ionization threshold (I_p) is 30.0 eV above the energy of the initial ground state for $R = 2.0$ bohr. The high-energy regime of photoelectron ATI peaks corresponding to up to 7-photon absorption can clearly be identified at such a high intensity. We notice that the results for the lowest few ATI peaks are already converged even when we truncate the expansion of the wave function at $|m|_{\max} = 4$. Higher-order angular momenta of $|m|_{\max} > 4$ still only have a minor effect in the high-energy regime, in which the ATI probability density is small. For the laser parameters considered here, the ATI spectrum is essentially converged even for absorption of as many as seven photons if only relatively small angular momenta are incorporated. In other words, the contributions from the channels with small angular momenta are still dominating the ATI peaks in the high-energy regime. The results presented below, therefore, were generated with $|m|_{\max} = 4$. This truncation is not expected to lead to any significant loss of numerical accuracy.

Figure 9 displays the ATI spectra from the weak intensity of 1×10^{13} W/cm^2 to the strong intensity of 1×10^{17} W/cm^2. At the lower intensities, for example, around 10^{15} W/cm^2, the n-photon absorption with $n \geqslant 2$ is very small (about 1/1000) compared to the dominant peak at the kinetic energy of 10 eV. In this intensity regime, therefore, the ionization is essentially a single-photon process. As expected, multiphoton absorption above the ionization threshold becomes more important as the intensity increases. Although the ATI "valleys" are not always evenly distributed around the ATI peaks, their separation clearly exhibits the energy quanta associated with the laser radiation. Equation (12) shows that the "area" enclosed by the ATI spectrum corresponds to the total ionization probability at the end of the laser interaction. Therefore, the ionization signal for n-photon absorption can be defined as the area between two ATI valleys with the ATI spectrum peaking at $n\omega_0 - I_p$. At the high intensity of 1×10^{17} W/cm^2, the contribution

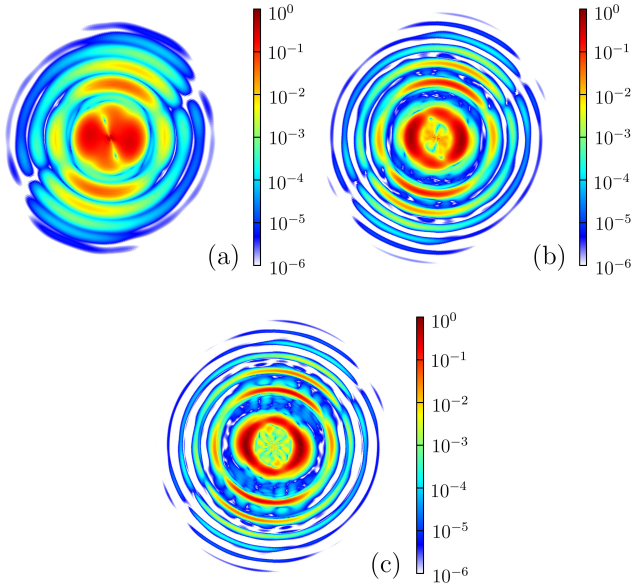

FIG. 10. (Color online) Momentum distribution $dP_{\rm ion}/d\boldsymbol{k}$ of the ATI spectra. The parameters of the elliptically polarized laser light are the same as in Fig. 8, except that the time scales are, respectively, 5 (a), 10 (b), and 15 optical cycles (c). The molecular axis is oriented along the vertical direction and the internuclear separation is $R = 2.0$ bohr. The color bar is given in the units defined as the density of ionization probability per unit volume of the three-dimensional momentum space, in which the momentum is in a.u.

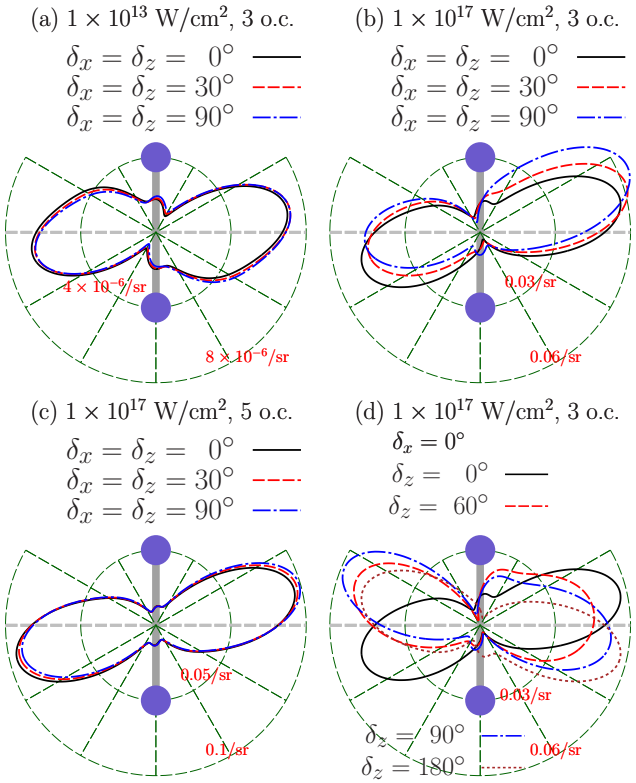

FIG. 11. (Color online) Angular distributions $dP_{\rm ion}/d\Omega$ for a central photon energy of 40 eV and pulse durations of 3 and 5 optical cycles. The peak intensities are 1×10^{13} W/cm^2 [(a)] and 1×10^{17} W/cm^2 [(b), (c), and (d)]. In panel (d) the phase δ_x is fixed at 0°, while $\delta_z = 0°$, 60°, 90°, and 180°, as indicated in the legend. The amplitudes of the electric field components are $E_0^x = 0.00844$, $E_0^z = 0.01462$ a.u. for $I_0 = 1 \times 10^{13}$ W/cm^2, and $E_0^x = 0.844$, $E_0^z = 1.462$ a.u. for $I_0 = 1 \times 10^{17}$ W/cm^2. The electric fields in panels (a)-(c) correspond to linearly polarized radiation, since the phases δ_x and δ_z are the same. The alignment angle between the polarization axis and the molecular axis is 30°.

to the ionization probability from the 1-photon process is 0.6279, while they are, respectively, 0.1397, 0.0311, and 0.0036 for 2-, 3-, and 4-photon absorption. This results in a total ionization probability of 0.8023 when the pulse is over after 1.55 fs. Note that the combination of the ponderomotive energy and the AC Stark shift of the ground state (they nearly compensate each other in this case) cause a small shift of the ATI peaks to the right with increasing laser peak intensity [c.f. Fig. 9(a)].

Fig. 9(b) addresses the question whether or not the present n-photon process ($1 \leqslant n \leqslant 7$) falls into the non-perturbative regime. For $I_0 \lesssim 5 \times 10^{16}$ W/cm^2, we see that the peaks of the ATI spectrum essentially follow the rule $\mathcal{P}_{\rm ion} \propto I_0^n$ from 1-photon to 7-photon absorption. For this photon energy, therefore, lowest-order perturbation theory is valid for multiphoton absorption in laser fields with peak intensities up to 5×10^{16} W/cm^2. Non-perturbative effects or higher-order corrections are only important for even higher intensities.

Furthermore, angular distributions of the ATI spectrum are unveiled through the momentum distributions, which are depicted in Fig. 10 for the peak intensity of 10^{17} W/cm^2 and pulse durations from "short" (5 o.c.) to "long" (15 o.c.). Beyond the expected narrowing of the widths of the ATI peaks, increasing the interaction time does not change the dominant emission mode even for multiphoton absorption. For single-photon absorption, the electron prefers to be emitted along the direction perpendicular to the molecular axis. For multi-photon absorption, however, it escapes mostly along the molecular axis.

Here we only discuss the angular distribution corresponding to single-photon absorption, i.e., the first ATI peak. For a peak intensity of 1×10^{17} W/cm^2, the angular distributions are obtained by collecting all ionization signals with kinetic energy less than 26.7 eV [c.f. Eqs. (11) and (12)]. This avoids any overlap with the second ATI peak. A detailed analysis of the angular distributions in the multiphoton regime will be presented in a separate publication.

If the interaction time of the H_2^+ ion with the laser pulse is as short as a few optical cycles, the calculated angular distributions may show significant deviations from those obtained for the long-puls cases. A strong intensity, combined with a short time scale, may add additional fla-

vor. In that case, the PADs can only be obtained by an explicitly time-dependent approach, and one may expect the results in very short pulses to become sensitive to the carrier envelope phases of the electric field components of the elliptically polarized radiation.

Even for a pulse duration as short as 310 attoseconds (3 cycles), Fig. 11(a) shows that the weak-field PADs at 40 eV photon energy are insensitive to the individual phases δ_x and δ_z, i.e., they only depend on the phase difference Δ. Figures 11(b) and (c), on the other hand, reveal a dependence on the individual phases δ_x and δ_z in the strong field of peak intensity $I_0 = 1\times10^{17}$ W/cm^2 for the same Δ. Depending on the details of the electric field, particularly the CEP, the angular distributions indicate that the photoelectron has a preferable direction for emission. The ionization patterns are not symmetric with respect to the molecular axis for a short pulse with strong intensity. In that case, the angular distributions can no longer be classified in terms of the phase difference between the two electric-field components. Instead, the effect of the individual "absolute" phases, i.e., the CEP effect, must be taken into account. These findings qualitatively agree with the conclusions of Pronin *et al.* [24] for the atomic case.

If the pulse duration increases, for example, to 517 as (5 cycles), the imparity in the dominant emission modes is almost smeared out. Further complexity in the PADs is observed in circularly ($\delta_x = 0°$ and $\delta_z = 90°$) and elliptically polarized ($\delta_x = 0°$ and $\delta_z = 60°$) radiation [c.f. Fig. 11(d)]. When the phase δ_x is fixed (at 0° in this example), varying δ_z generally results in the PAD oscillating between the two sets of linearly polarized lasers ($\delta_z = 0°$ and $\delta_z = 180°$).

For few-cycle pulses, the spatial box of $\xi_{\max} = 400$ is sufficiently large to fit the electronic wave packet for the entire time. No artificial reflection at the edge was observed. The above results can be reproduced in a large box of $\xi_{\max} = 521$. Therefore, changes in the angular distributions at 1×10^{17} W/cm^2 should be attributed to the strong-field effect. Though the ponderomotive energy U_p is still less than the ionization energy, its effect may not be negligible. For example, in the case of linearly polarized radiation, U_p is 8.97 eV and the Keldysh parameter is 1.3 for the laser parameters used in Fig. 11(b). Although this scenario may still fall into the multiphoton regime, the Keldysh parameter being so close to unity makes the contributions from channels with high angular momenta not negligible even at the equilibrium separation.

IV. SUMMARY AND CONCLUSIONS

We have explored the photoionization of the H_2^+ molecular ion irradiated by elliptically polarized laser pulses at photon energies ranging from 40 eV to 300 eV. The TDSE was formulated in two-center prolate spheroidal coordinates in the fixed-nuclei approximation and solved for two initial states, $1s\sigma_g$ and $2p\sigma_u$, respectively. Exact continuum states of the system were used to extract the cross sections and the photoelectron angular distributions. We found that the confinement effect observed in linearly polarized radiation persists for elliptically polarized lasers. The asymmetric rotational effect is most noticeable for near-threshold ionization. The rotational effect and the dichroism were explained by analyzing the various contributions to the predicted cross sections. Coupling the rotational and confinement effects significantly complicates the angular distributions compared to linearly polarized lasers.

As expected, the angular distributions obtained from short and intense pulses are sensitive to the individual carrier-envelope phases. The question remains whether or not a decomposition of the PADs in terms of l and ζ, similar to the one suggested here for sufficiently long pulses, exists for very short pulses as well. Furthermore, it seems worthwhile to examine a possible confinement, if it exists, in such a scenario. These topics will be the subject of future work in our group.

ACKNOWLEDGMENTS

This work was supported by the United States National Science Foundation under grant No. PHY-1068140 and by the XSEDE allocation No. PHY-090031.

Appendix: Polarization vector

We define the xz-plane as the polarization plane with the unit vectors $\boldsymbol{e}_x$ and $\boldsymbol{e}_z$ along the x- and z-axes, respectively. For an arbitrary elliptical light polarization, the electric field is given in Eqs. (6) and (7). Apparently, the polarization vector $\boldsymbol{\epsilon}$ cannot be a real vector for arbitrarily polarized light. A real vector $\boldsymbol{\epsilon}$ is only possible for linearly polarized light. The complex polarization vector can be further written as

$$\boldsymbol{\epsilon} = \frac{\hat{\boldsymbol{\epsilon}}_R + i\epsilon_I\hat{\boldsymbol{\epsilon}}_I}{\sqrt{1+\epsilon_I^2}} \tag{24}$$

for an elliptically polarized electric field. Here $\hat{\boldsymbol{\epsilon}}_R$ and $\hat{\boldsymbol{\epsilon}}_I$ denote the unit vectors of the real and imaginary parts, respectively, which are perpendicular to each other. The above polarization vector is normalized according to $\boldsymbol{\epsilon}\cdot\boldsymbol{\epsilon}^* = 1$. In Ref. [28], the determination of the major and minor axes of the ellipse is discussed. Here we show the details of how these two axes are associated with the polarization vector.

We assume that the angle between $\hat{\boldsymbol{\epsilon}}_R$ and $\boldsymbol{e}_x$ is ϕ, and hence it is $\phi+\pi/2$ between $\hat{\boldsymbol{\epsilon}}_I$ and $\boldsymbol{e}_x$. After introducing $\tilde{a} = \mathcal{E}_0/\sqrt{1+\epsilon_I^2}$ and $\tilde{b} = \mathcal{E}_0\epsilon_I/\sqrt{1+\epsilon_I^2}$, we have

$$E_0^x\cos(\omega_0 t+\delta_x) = \tilde{a}\cos\phi\cos(\omega_0 t+\delta) - \tilde{b}\sin\phi\sin(\omega_0 t+\delta) \tag{25}$$

and

$$E_0^z \cos(\omega_0 t + \delta_z) = \tilde{a} \sin\phi \cos(\omega_0 t + \delta) + \tilde{b} \cos\phi \sin(\omega_0 t + \delta) \quad (26)$$

at any time t. This yields

$$\tilde{a} \sin\delta = E_0^x \cos\phi \sin\delta_x + E_0^z \sin\phi \sin\delta_z, \quad (27)$$
$$\tilde{a} \cos\delta = E_0^x \cos\phi \cos\delta_x + E_0^z \sin\phi \cos\delta_z, \quad (28)$$
$$\tilde{b} \sin\delta = -E_0^x \sin\phi \cos\delta_x + E_0^z \cos\phi \cos\delta_z, \quad (29)$$
$$\tilde{b} \cos\delta = E_0^x \sin\phi \sin\delta_x - E_0^z \cos\phi \sin\delta_z. \quad (30)$$

Therefore,

$$\tilde{a}^2 = (E_0^x)^2 \cos^2\phi + (E_0^z)^2 \sin^2\phi + E_0^x E_0^z \sin(2\phi) \cos\Delta, \quad (31)$$

and

$$\tilde{b}^2 = (E_0^x)^2 \sin^2\phi + (E_0^z)^2 \cos^2\phi - E_0^x E_0^z \sin(2\phi) \cos\Delta. \quad (32)$$

Manipulating the above two equations shows that $\mathcal{E}_0 = \sqrt{(E_0^x)^2 + (E_0^z)^2}$, which is related to one of Stokes parameters through $\mathcal{E}_0^2 = s_0$ [28]. Hence, $\mathcal{E}_0^2$ is essentially proportional to the peak intensity of the laser pulse, which depends on both components of the electric field. To determine the angle ϕ, we need to separate the discussions for circular and elliptical (i.e., non-circular) polarized radiation. The phase difference $\Delta = \delta_z - \delta_x$ will be used in the discussion below.

Circularly polarized light. In this case, we have $E_0^x = E_0^z$, $\Delta = \pm\pi/2$, and therefore $\epsilon_I = \pm 1$. We see that any angle ϕ can satisfy Eqs. (31) and (32) for circularly polarized light, and thus we choose $\phi = 0$ without loss of generality.

Next we set up the correspondence between the signs of Δ and ϵ_I. To begin with, $\delta = \delta_x + 2\pi l_x$ from the x component of the electric field. Also, $\delta = \pi/2 + 2\pi l_z + \delta_z$ if $\epsilon_I = +1$, and $\delta = -\pi/2 + 2\pi l_z + \delta_z$ if $\epsilon = -1$ follow from the z component of the field. Both l_x and l_z are integer numbers. This yields the phase difference

$$\Delta = -\pi/2 + 2\pi(l_x - l_z) = -\pi/2 \ \text{ if } \epsilon_I = +1, \quad (33)$$

$$\Delta = \pi/2 + 2\pi(l_x - l_z) = \pi/2 \ \text{ if } \epsilon_I = -1. \quad (34)$$

Without loss of generality, $2\pi(l_x - l_z)$ can be dropped since only $\sin\Delta$ and $\cos\Delta$ are needed. Therefore, the polarization vector is given by $\boldsymbol{\epsilon} = (\boldsymbol{e}_x \pm i\boldsymbol{e}_z)/\sqrt{2}$ for circularly polarized electric fields. Figure 12 shows the temporal rotation for $\Delta = +\pi/2$ and $-\pi/2$ in the given coordinate system $\boldsymbol{e}_x$-$\boldsymbol{e}_z$. Here we have clockwise and anti-clockwise rotation, respectively, for $\Delta = +\pi/2$ and $\Delta = -\pi/2$.

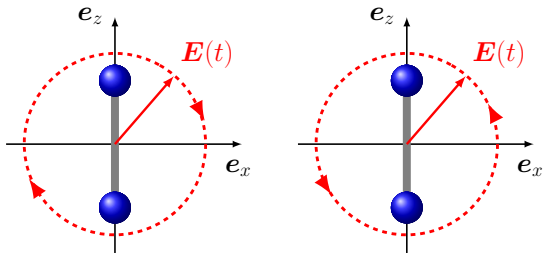

(a) $\Delta = +\pi/2$ (b) $\Delta = -\pi/2$

FIG. 12. (Color online) Circularly polarized light with phase differences $\Delta = +\pi/2$ (a) and $\Delta = -\pi/2$ (b). The molecular axis is along the vertical direction.

Elliptical (non-circular) polarized light. In this case, the phase δ satisfies

$$\tan\delta = \frac{E_0^x \cos\phi \sin\delta_x + E_0^z \sin\phi \sin\delta_z}{E_0^x \cos\phi \cos\delta_x + E_0^z \sin\phi \cos\delta_z} = \frac{-E_0^x \sin\phi \cos\delta_x + E_0^z \cos\phi \cos\delta_z}{E_0^x \sin\phi \sin\delta_x - E_0^z \cos\phi \sin\delta_z}. \quad (35)$$

We obtain

$$\tan(2\phi) = \frac{2E_0^x E_0^z}{(E_0^x)^2 - (E_0^z)^2} \cos\Delta, \quad (36)$$

which only depends on the amplitude ratio E_0^z/E_0^x and the phase difference Δ. Apparently, $\tan(2\phi) = s_2/s_1$ in terms of the Stokes parameters s_1 and s_2 [28].

Note that Eq. (36) is not valid for circularly polarized light. The angle ϕ may, in principle, take up multiple values. For example, if the angle ϕ satisfies Eq. (36), then $\phi \pm \pi/2$ and $\phi \pm \pi$ are solutions as well. This corresponds to four directions, which are either orthogonal or antiparallel to each other. This indicates that both angles for the directions of $\hat{\boldsymbol{\epsilon}}_R$ and $\hat{\boldsymbol{\epsilon}}_I$ satisfy the same equation (36). Furthermore, it also means that the directions of $\hat{\boldsymbol{\epsilon}}_R$ and $\hat{\boldsymbol{\epsilon}}_I$ are interchangeable. Physically, we may choose any of them as the direction $\hat{\boldsymbol{\epsilon}}_R$ and then perform an anticlockwise rotation by $\pi/2$ to obtain the direction of $\hat{\boldsymbol{\epsilon}}_I$. In practice, without loss of generality, we can choose the angle ϕ in such a way that $|\tilde{a}| \geqslant |\tilde{b}|$. Consequently, $|\epsilon_I| \leqslant 1$. In this way, ϵ_I is the ellipticity of the polarization ellipse. Comparing with the shape and size parameters of the polarization ellipse, we recognize that $\hat{\boldsymbol{\epsilon}}_R$ and $\hat{\boldsymbol{\epsilon}}_I$ are along the *major* and *minor* axes of the ellipse, respectively. Furthermore, $|a|$ and $|b|$ are the lengths of the semi-major and semi-minor axes. Finally, once we define the angle $\phi = 0$ for circularly polarized light, we can carry out a unified discussion for arbitrarily polarized electric fields.

Elliptically polarized light. Even though we know the directions of $\hat{\boldsymbol{\epsilon}}_R$ and $\hat{\boldsymbol{\epsilon}}_I$, ϵ_I remains to be determined. Note that ϵ_I could take up a positive, negative, or zero value, which needs to be compatible with our convention

of $\hat{\boldsymbol{\epsilon}}_I$. Generally, we have

$$\epsilon_I = \frac{\tilde{b}}{\tilde{a}} = \frac{-E_0^x \sin\phi\cos\delta_x + E_0^z \cos\phi\cos\delta_z}{E_0^x \cos\phi\sin\delta_x + E_0^z \sin\phi\sin\delta_z} \tag{37}$$

$$= \frac{E_0^x \sin\phi\sin\delta_x - E_0^z \cos\phi\sin\delta_z}{E_0^x \cos\phi\cos\delta_x + E_0^z \sin\phi\cos\delta_z}. \tag{38}$$

For circularly polarized light, in particular, $E_0^x = E_0^z$, $\Delta = \pm\pi/2$, and $\phi = 0$. The above equation then reduces to $\epsilon_I = -1$ if $\Delta = +\pi/2$ and $\epsilon_I = +1$ if $\Delta = -\pi/2$, in agreement with what we derived before. If one of the amplitudes vanishes, it reduces to linearly polarized light. Linearly polarized light also occurs when $\Delta = l\pi$ ($l = 0, \pm1, \pm2, \ldots$), even when both amplitudes are different from zero. In this case, the angle ϕ (with respect to $\boldsymbol{e}_x$) can be determined by $\phi = \tan^{-1}(E_0^z/E_0^x)$ for even l and $\phi = -\tan^{-1}(E_0^z/E_0^x)$ for odd l.

At first sight, Eq. (38) might suggest that the ellipticity ϵ_I depends on δ_x and δ_z, individually, in addition to its dependence on the amplitude ratio E_0^z/E_0^x. Further derivation, however, shows that

$$\epsilon_I = \frac{|b|}{|a|}\sin(\beta_b - \beta_a), \tag{39}$$

in which the auxiliary angles β_a and β_b are given by

$$\beta_a = \tan^{-1}\left[\frac{-E_0^z \sin\phi\sin\Delta}{E_0^x\cos\phi + E_0^z\sin\phi\cos\Delta}\right] + (0 \text{ or } \pi), \tag{40}$$

$$\beta_b = \tan^{-1}\left[\frac{-E_0^z \cos\phi\sin\Delta}{-E_0^x\sin\phi + E_0^z\cos\phi\cos\Delta}\right] + (0 \text{ or } \pi). \tag{41}$$

The additional angle of either 0 or π is determined by the signs of the denominators in the brackets. The angle is 0 if the denominator $\geqslant 0$ and π otherwise. Note that $\sin(\beta_b - \beta_a) = \pm1$.

At this point, we recognize that the polarization vector $\boldsymbol{\epsilon}$ is only determined by the amplitude ratio E_0^z/E_0^x and the phase difference Δ. It is independent of the individual values for E_0^x, E_0^z, δ_x, and δ_z.

[1] L. Young, E. P. Kanter, B. Krassig, Y. Li, A. M. March, S. T. Pratt, R. Santra, S. H. Southworth, N. Rohringer, L. F. DiMauro, G. Doumy, C. A. Roedig, N. Berrah, L. Fang, M. Hoener, P. H. Bucksbaum, J. P. Cryan, S. Ghimire, J. M. Glownia, D. A. Reis, J. D. Bozek, C. Bostedt, and M. Messerschmidt, Nature, **466**, 56 (2010).

[2] P. R. Ribic and G. Margaritondo, J. Phys. D **45**, 213001 (2012).

[3] D. Akoury, K. Kreidi, T. Jahnke, Th. Weber, A. Staudte, M. Schöffler, N. Neumann, J. Titze, L. Ph. H. Schmidt, A. Czasch, O. Jagutzki, R. A. Costa Fraga, R. E. Grisenti, R. Díez Muiño, N. A. Cherepkov, S. K. Semenov, P. Ranitovic, C. L. Cocke, T. Osipov, H. Adaniya, J. C. Thompson, M. H. Prior, A. Belkacem, A. L. Landers, H. Schmidt-Böcking, and R. Dörner, Science, **318**, 949 (2007).

[4] D. A. Horner, S. Miyabe, T. N. Rescigno, C. W. McCurdy, F. Morales, and F. Martín, Phys. Rev. Lett. **101**, 183002 (2008).

[5] D. Rolles, M. Braune, S. Cvejanović, O. Gebner, R. Hentges, S. Korica, B. Langer, T. Lischke, G. Prümpler, A. Reinköster, J. Viefhaus, B. Zimmermann, V. McKoy, and U. Becker, Nature, **437**, 711 (2005).

[6] J. Fernández, F. L. Yip, T. N. Rescigno, C. W. McCurdy, and F. Martín, Phys. Rev. A **79**, 043409 (2009).

[7] J. Fernández, O. Fojón, A. Palacios, and F. Martín, Phys. Rev. Lett. **98**, 043005 (2007).

[8] X. Guan, E. B. Secor, K. Bartschat, and B. I. Schneider, Phys. Rev. A **85**, 043419 (2012).

[9] X. Guan, E. B. Secor, R. C. DuToit, and K. Bartschat, Phys. Rev. **86**, 053425 (2012).

[10] V. V. Strelkov, M. A. Khokhlova A. A. Gonoskov, I. A. Gonoskov, and M. Yu. Ryabikin, Phys. Rev. A **86**, 013404 (2012).

[11] G. Sansone, E. Benedetti, F. Calegari, C. Vozzi, L. Avaldi, R. Flammini, L. Poletto, P. Villoresi, C. Altucci, R. Velotta, S. Stagira, S. De Silvestri, and M. Nisoli, Science, **314**, 443 (2006).

[12] H. D. Cohen and U. Fano, Phys. Rev. **150**, 30 (1966).

[13] I. G. Kaplan and A. P. Markin, Sov. Phys. Dokl. **14**, 36 (1969).

[14] K.-J. Yuan and A. D. Bandrauk, Phys. Rev. A **85**, 053419 (2012).

[15] X. Guan, E. B. Secor, K. Bartschat, and B. I. Schneider, Phys. Rev. A **84**, 033420 (2011).

[16] X. Guan, K. Bartschat, and B. I. Schneider, Phys. Rev. A **84**, 033403 (2011).

[17] X. Guan, K. Bartschat, and B. I. Schneider, Phys. Rev. A **83**, 043403 (2011).

[18] E. Hecht and A. Zajac, *Optics*, Chap. 8, (Addison-Wesley Publishing, Reading, 1979).

[19] R. P. Feynman, R. B. Leighton, and M. Sands, *The Feynman Lectures on Physics*, Chap. 33, (single volume, Basic Books, New York, 2013).

[20] N. L. Manakov, A. Maquet, S. I. Marmo, V. Veniard, and G. Ferrante, J. Phys. B **32**, 3747 (1999).

[21] A. V. Flegel, M. V. Frolov, N. L. Manakov, A. F. Starace, and A. N. Zheltukhin, Phys. Rev. **A** 87, 013404 (2013).

[22] X. Guan, K. Bartschat, and B. I. Schneider, Phys. Rev. A **82**, 041404 (2010).

[23] B. I. Schneider, J. Segura, A. Gil, X. Guan, and K. Bartschat, Comput. Phys. Comm. **181**, 2091 (2010).

[24] E. A. Pronin, A. F. Starace, M. V. Frolov, and N. L. Manakov, Phys. Rev. A **80**, 063403 (2009).

[25] E. A. Pronin, N. L. Manakov, S. I. Marmo, and A. F. Starace, J. Phys B **40**, 3115 (2007).

[26] X. Guan, C. J. Noble, O. Zatsarinny, K. Bartschat, and B. I. Schneider, Comput. Phys. Comm. **180**, 2401 (2009).
[27] M. Walter and J. Briggs, J. Phys. B **32**, 2487 (1999).
[28] M. Born and E. Wolf, *Principles of Optics*, Chap. 1, (4th edition, Pergamon Press, 1970).